JOURNAL OF SOLID STATE CHEMISTRY 92, 8–17 (1991)

Electronic Properties of $Na_{0.33}V_2O_5$ Bronze Obtained by the Sol–Gel Process

J. C. BADOT, D. GOURIER, F. BOURDEAU, N. BAFFIER, AND A. TABUTEAU*

*Laboratoire de Chimie Appliquée de l'Etat Solide (URA 302 CNRS), Ecole Nationale Supérieure de Chimie de Paris; and *Institut Curie (URA 448 CNRS), 11 rue P. et M. Curie 75231 Paris Cedex 05 France*

Received July 27, 1990

Studies on magnetic susceptibility, electron paramagnetic resonance, electrical conductivity, and dielectric relaxation measurements of β-$Na_{0.33}V_2O_5$ bronze powders and films obtained by the sol–gel process are presented. According to magnetic susceptibility measurements, the V^{4+} ions occupy 56% of the V_1 sites and 11% of the V_3 sites and it is shown by EPR studies that the bipolaron model describes the electronic properties of the bronze as in the case of the bronze obtained by solid state reaction. Electrical conductivity and dielectric relaxation measurements have also shown that this method of preparation does not affect the electronic transport properties, which can be interpreted in terms of a collective motion of bipolarons with a correlation time of 10^{-11} sec.

Introduction

The preparation of materials (e.g., ceramics and glasses) by the sol–gel process has aroused much interest in recent years. Gel routes offer specific advantages to prepare fine powders or thin films leading to well-densified ceramics or orientated layers. New morphologies can be obtained and new physical properties depending on the structure are expected. Particularly, the rheological properties of sols or gels allow the obtaining of fibers or films with enhanced anisotropy and chemical reactivity. It is possible to obtain by this route monoclinic bronzes $Na_{0.33}V_2O_5$ from vanadium oxide gels with a ribbon structure close to that of orthorhombic V_2O_5 oxide (*1*).

The bronze obtained by the sol–gel process (hereafter referred to as SGP bronze) was shown to be promising as a rechargeable cathodic material in secondary lithium cells (*2*). For use, the knowledge of the physical properties of SGP bronze, especially conductivity mechanisms, is necessary. Our purpose is to discuss these properties by comparing them with those of the same material obtained by solid state reaction (hereafter referred to as SSR bronze). For this purpose, we have studied the effect of the synthesis method on the magnetic and electrical properties by using the following techniques: magnetic susceptibility, electron paramagnetic resonance (EPR), electrical conductivity, and dielectric relaxation measurements (*3*).

The vanadium oxide bronzes $M_xV_2O_5$ were synthesized for the first time by Hautefeuille (*4*), and much later investigated by Hagenmuller *et al.* in the 1970s (*5–7*). These

0022-4596/91 $3.00

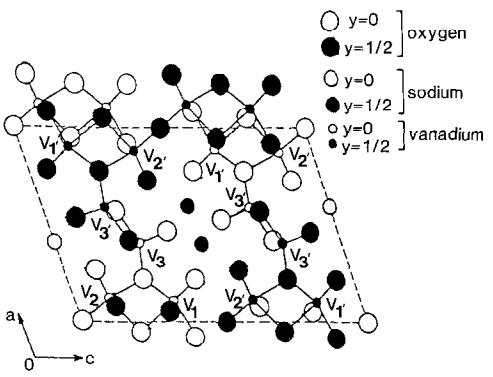

FIG. 1. Projection in the (a,c) plane of the atomic positions in the monoclinic $Na_{0.33}V_2O_5$ bronze.

compounds were obtained by solid state reaction of different oxides at 650°C for 1 or 2 days under argon flux.

The crystal structure of NaV_6O_{15} (β-$Na_{0.33}V_2O_5$) was found to be monoclinic, space group: $A2/m$, $Z = 2$ and $a = 10.08$ Å, $b = 3.61$Å, $c = 15.44$Å, $\beta = 109.6°$. The projection of the structure on the (a,c) plane is shown on Fig. 1 (after Ref. (*8*)). The structure consists of zig–zag double strings of VO_6 octahedra forming sheets parallel to the (a,c) plane. Adjacent sheets are joined by additional chains parallel to the b axis. These chains are made of double VO_5 trigonal bipyramids giving rise to the tunnel structure. The vanadium sites are V_1 and V_2 for octahedral sites and V_3 for the center of the trigonal bipyramids. After Goodenough (*9*), the V^{4+} ions occupy 50% of the V_1 sites, and few of the V_3 sites. In the (a,c) plane projection (cf. Fig. 1), each tunnel contains two interstitial equivalent sites labeled M_1 and M_1'. The Na^+ ions are equally distributed between these sites. Consequently, the structure of vanadium oxide bronze $Na_{0.33}V_2O_5$ is very anisotropic, which leads to quasi-one-dimensionality for electrical properties. The conductivity is of the semiconductor type along the b axis and is two orders of magnitude higher than that measured in the (a,c) plane (*10*).

In the case of SSR bronze (β-$Na_{0.33}V_2O_5$), ^{23}Na NMR (*11*) has shown that the resonance line has zero Knight shift, which indicates that sodium atoms have donated the outer s electron to the d orbital of the vanadium atom. The majority of the donated 0.33 electrons occupy the vanadium position at V_1 sites (*9*). Thus, vanadium ions are found in both $V^{4+}$and V^{5+} states. X-ray diffraction studies below 200 K (*12*) show that the structure is constituted by V^{4+}–V^{4+} dimers, which results in the formation of these pairs along zig–zag chains parallel to the b axis. In the bipolaron model proposed by Chakraverty *et al.* (*13*), the dimer V^{4+}–V^{4+} has a spin singlet ground state, and the first excited state of the bipolaron is a triplet state (Fig. 2). However, the "dissociation energy" 2Δ of the bipolaron is smaller than the singlet–triplet exchange energy $2J$, and thus the triplet state of the bipolaron is not thermally accessible. By magnetic susceptibility measurements, it is possible to determine the unpaired electron occupancy of the V_1 and V_3 sites and 2Δ, the energy separation between the singlet ground state of the bipolaron and the ground state of isolated polarons. In principle, we can also determine by EPR the interaction between magnetic spins and the hyperfine interaction with ^{51}V nuclei. In the first part, these two techniques are used to compare the magnetic properties

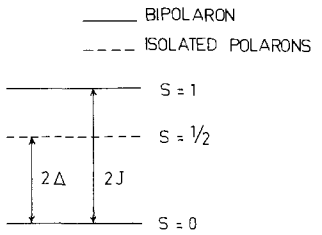

FIG. 2. Schematic representation of the two lowest spin states of bipolarons and of the isolated polaron state. 2J and 2Δ are respectively the singlet–triplet exchange energy and the dissociation energy of the bipolaron.

of SGP and SSR bronzes (*11, 13–15*). The electrical conductivities of the two types of bronzes are then compared.

Experimental

Vanadium oxide gels synthesized by polycondensation of vanadic acid correspond to the formula V_2O_5, nH_2O. Following the value of n, a gel ($n < 300$) or a colloidal solution ($n > 300$) is obtained. By drying at room temperature, a xerogel with the composition V_2O_5, 1.6 H_2O is formed (*16*). Transmission electron microscopy (TEM) observations show that the xerogel is composed of flat and ribbon-shaped entangled fibers having the dimensions $10 \times 10^2 \times 10^3 Å^3$ (*17*) and with a structure close to that of orthorhombic V_2O_5 (*18*). If a layer of the xerogel is deposited on a glass plate, its X-ray diffraction pattern in reflection geometry is typical of a layered structure resulting from the parallel arrangement of the ribbons on the substrate. The basic distance is d = 11.5 Å. Consequently, the anisotropic structure of the orthorhombic V_2O_5 is enhanced by this method. The V_2O_5, 1.6 H_2O xerogel, which behaves as a layered host structure, can easily intercalate ionic species (e.g., Na^+, K^+, Li^+, . . .) by immersion of the sample in an aqueous solution of the corresponding chloride for a few minutes (*19, 20*). When the exchange is achieved in the case of the Na^+ ion, the resulting xerogel has the formula $Na_{0.33}V_2O_5$, 1.6 H_2O, corresponding to a basic distance d = 10.9 Å. After evaporation of all water content at 550°C, this xerogel gives rise to the $Na_{0.33}V_2O_5$ bronze (*1, 21*). In order to compare this SGP bronze and the usual SSR bronze, X-ray diffraction patterns (*1, 21*) were performed in reflection geometry thin film and powder in the case of SGP bronze. The two compounds are monoclinic and the parameters of the SGP bronze (a = 10.10 ± 0.05 Å, b = 3.63 ± 0.01 Å, c = 15.15 ± 0.05 Å, β = 110.0 ± 0.5°) are close to those of the SSR bronze. Only the Braggs peaks 002, 004, 104, and 106 appear with noticeable intensities on the diffraction pattern of the SGP bronze in reflexion geometry (Fig. 3). This corresponds to an alignment of the tunnels of the structure over large domains parallel to the (a,b) plane.

Magnetic susceptibility measurements were performed on SGP bronze powder with a Faraday electrobalance in the temperature range 4 to 300 K. The temperature was measured using an Au (0.07 Fe)–Chromel thermocouple located near the sample. The uncertainty of the sample temperature is ±0.5 K after calibration.

EPR spectra were recorded on a Bruker 220D spectrometer operating at X-band and equipped with the variable temperature accessory (100 to 300 K). Low temperatures (4 to 100 K) were obtained with an helium flow cryostat ESR9 from Oxford Instrument. The magnetic field and the microwave frequency were measured with a Gaussmeter and frequency meter.

Conductivity measurements were performed between 40 and 300 K with dc-technique on SGP bronze film in directions parallel and perpendicular to the film surface. Gold electrodes were deposited on the film in order to ensure good electrical contacts. Dielectric relaxation measurements (*3*) were performed in the temperature range 240–300 K, between 1 MHz and 10 GHz using an HP4191A impedance meter and an HP8410 network analyzer. The cell is a special circular coaxial line whose inner conductor is interrupted by the sample pellet. The full apparatus was described elsewhere (*22, 23*).

Results and Discussion

Magnetic Susceptibility

In the bronze β-$Na_{0.33}V_2O_5$, only isolated polarons with electron spin S = 1/2 contribute to the magnetic susceptibility χ, since

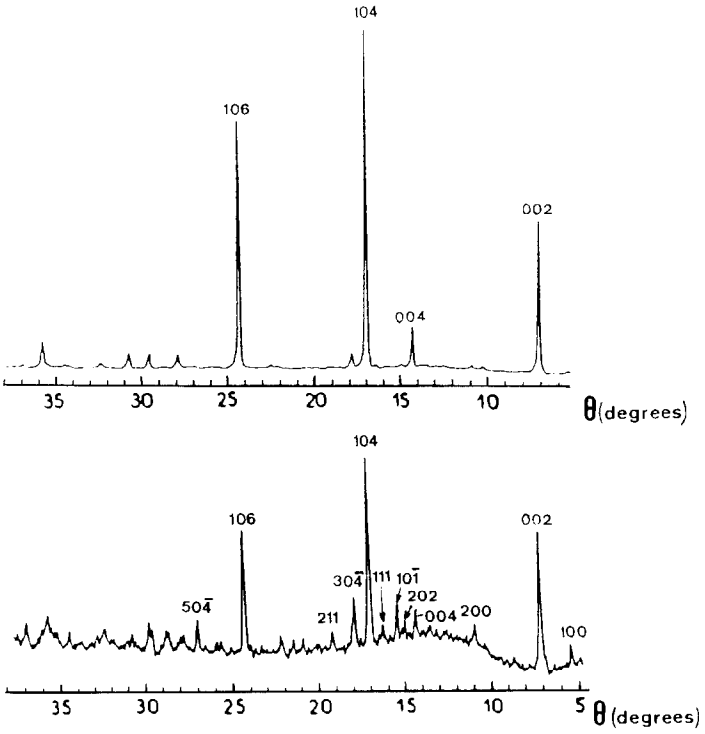

FIG. 3. X-ray diffraction spectra (reflection geometry, λ Cu$K\alpha$) of SGP bronze: (a) film; (b) powder.

the other species (V^{5+}, Na^+, O^{2-}, bipolarons in the singlet state) have zero electron spin. Thus the presence of bipolarons can only be due to their dissociation into isolated polarons under the effect of thermal agitation. If n_{pol} and n_{bip} are respectively the fraction of polarons and bipolarons, n_{pol} will increase with temperature as $n_{pol} = n_{bip} \exp(-\Delta/kT)$. Taking into account the conservation of the total number of polarons $n_{pol} + n_{bip} = 1$, we obtain $n_{pol} = \exp(-\Delta/kT) \cdot [1 + \exp(-\Delta/kT)]^{-1}$ and $n_{bip} = [1 + \exp(-\Delta/kT)]^{-1}$. The increase of n_{pol} with T should result in two effects: to induce a positive deviation of the magnetic susceptibility from the Curie–Weiss law, and to decrease the mean distance between isolated polarons. The former effect can be accurately studied by magnetic susceptibility measurement, and the latter by EPR. Returning to magnetic susceptibility, it should be possible to distinguish between:

(i) the polarons at V_1 sites resulting from the thermal dissociation of singlet bipolarons, whose susceptibility is given by the expression

$$\chi_1 = (C_1/T) \exp(-\Delta/kT)/[1 + \exp(-\Delta/kT)],$$

where $C_1$is the Curie constant.

(ii) isolated polarons at V_3 sites, whose number is not temperature dependent, so that their magnetic susceptibility χ_3 follows a simple Curie–Weiss law, $\chi_3 = C_3/(T + \theta_p)$, where C_3 and θ_p are the Curie–Weiss constant and the Curie paramagnetic temperature, respectively.

Consequently, the total susceptibility, χ, associated to polarons at V_1 and V_3 sites is

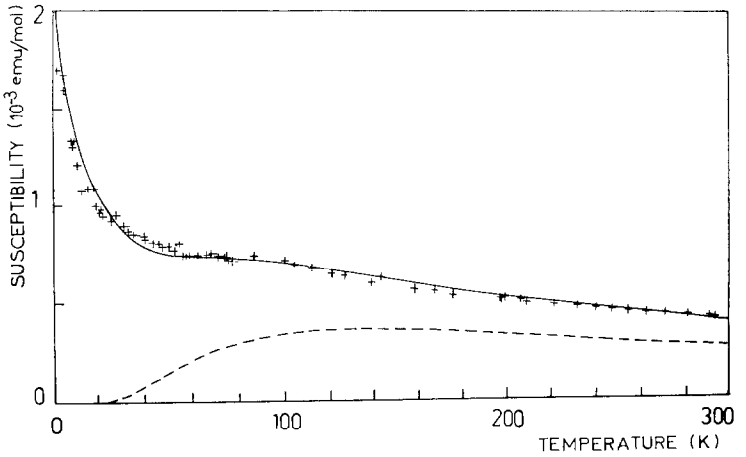

FIG. 4. Temperature dependence of the magnetic susceptibility of SGP bronze. The dashed line represents the susceptibility due to polarons at the V_1 site and the full line represents the sum of the contributions of polarons at V_1 and V_3 sites.

expressed as the sum of these two contributions:

$$\chi = (C_1/T)\exp(-\Delta/kT)/[1 + \exp(-\Delta/kT)] + C_3/(T + \theta_p). \quad (1)$$

At very low temperatures, i.e., $T = 4$ K, all the bipolarons are in the $S = 0$ state and are not dissociated. Thus the susceptibility, χ, is only due to polarons at V_3 sites, i.e., $\chi = \chi_3$.

Figure 4 shows the temperature dependence of the magnetic susceptibility of SGP bronze between 4 K and the room temperature. It is evident that χ follows a Curie–Weiss behavior below 30 K, due to isolated polarons at V_3 sites. Consequently the deviation from the Curie–Weiss law at higher temperatures is due to the contribution of the dissociated bipolarons.

It is then possible to determine the different parameters C_1, C_3, θ_p, and Δ by fitting our experimental results to Expression (1). The results are given in Table I. The proportion $[V^{4+}]_i$ of V^{4+} ions at site V_i is expressed by:

$$[V^{4+}]_i = C_i/\Sigma_i C_i, \ (i = 1, 3).$$

Consequently, 84 and 16% of V^{4+} are found at V_1 and V_3 sites, respectively (cf. Table I). It should be noticed that the parameters θ_c, Δ, and $[V^{4+}]_i$ in SGP and SSR (*11*) bronzes are nearly identical.

EPR Measurements

EPR spectroscopy allows as to detect isolated polarons at V_1 and V_3 sites. The triplet

TABLE I

PARAMETERS DEDUCED FROM MAGNETIC SUSCEPTIBILITY MEASUREMENTS

Parameters	SGP Bronze[a]	SSR Bronze[b]
C_1 (emuK/mole)	0.223	0.133
C_3 (emuK/mole)	0.042	0.029
θ_c (K)	20	18
Δ/k (K)	168	169
% V^{4+} in V_1 site	84	82
% V^{4+} in V_3 site	16	18

Note. SGP and SSR bronzes are respectively obtained by the sol–gel process and by solid-state reactions. C_1, C_3, θ_c, Δ/k, and V^{4+} concentration in V_1 and V_3 sites are calculated from expression 1.

[a] This work.

[b] Ref. (*11*).

state ($S = 1$) of bipolarons should give rise to a characteristic EPR spectrum, but this state is not thermally accessible since the dissociation energy 2Δ of the bipolaron is lower than the exchange energy $2J$. Figure 5a shows the X-band EPR spectrum at 140° K of a SGP bronze powder. It does not exhibit the expected hyperfine pattern due to the ^{51}V ($I = 7/2$) nucleus, and is composed only of a broad line with an apparent structure near its center. This spectrum is accurately simulated by the sum of two single lines with Lorentzian shapes: an intense one centered at $g = 1.964$, and a narrow one centered at $g = 1.979$. Their respective surfaces, S, can be estimated by the expression $S = h\,(\Delta B)^2$, where h is the peak to peak amplitude and ΔB is the peak to peak linewidth. The surface of the narrow line is only 0.6% that of the broad line. The g factor of the broad line is very close to the average value $g_{av} = 1/3(g_x + g_y + g_z) = 1.961$ for the polaron at the V_1 site in SSR bronze (*14*), with $g_x = 1.930$, $g_y = 1.969$, and $g_z = 1.983$. The EPR spectra at 110 K of SGP films are shown in Figs. 5b and 5c for two orientations of the film surface with respect to the magnetic field B. In both cases, the spectra can be simulated by the sum of one broad and one narrow line with Lorentzian shapes and with different amplitudes and widths. The g factor of the narrow line does not depend significantly on the film orientation since the two components are $\langle g_{\parallel} \rangle = 1.970$ and $\langle g_{\perp} \rangle = 1.983$ when B is respectively perpendicular ($\theta = 0$) and parallel ($\theta = \pi/2$) to the film surface. On the contrary, the g factor of the broad line is more orientation dependent. The g values are $\langle g_{\parallel} \rangle = 1.940$ and $\langle g_{\perp} \rangle = 1.964$ for $\theta = 0$ and $\theta = \pi/2$, respectively. Since the broad line is essentially due to polarons at V_1 sites, the apparent anisotropy of the g factor reflects the partial orientations of the film observed on X-ray diffraction patterns. In SGP films, the relative surface of the narrow line is smaller than in SGP powders, since it represents only 0.2% of the surface of the broad line in that case. Therefore, this narrow line spectrum will not be considered further and we shall focus our attention on the broad line spectrum attributed to isolated polarons. It is noteworthy that this line does not exhibit the hyperfine pattern due to the ^{51}V ($I = 5/2$) nucleus. This fact, and the Lorentzian shape of the line in the entire temperature range (4 to 300 K) shows that we are dealing with the extreme motional narrowing regime (*24*). Under this condition, the EPR linewidth ΔB is given by:

$$\Delta B = (\langle \omega_{hf}^2 \rangle + \langle \omega_{dip}^2 \rangle)\,\tau_c,$$

where $\langle \omega_{hf}^2 \rangle$ and $\langle \omega_{dip}^2 \rangle$ are respectively the second moments due to unresolved hyperfine interaction and to dipolar interactions between polarons. The correlation time for electron hopping $\tau_c = 10^{-11}$ sec is assumed to be temperature independent, as shown in

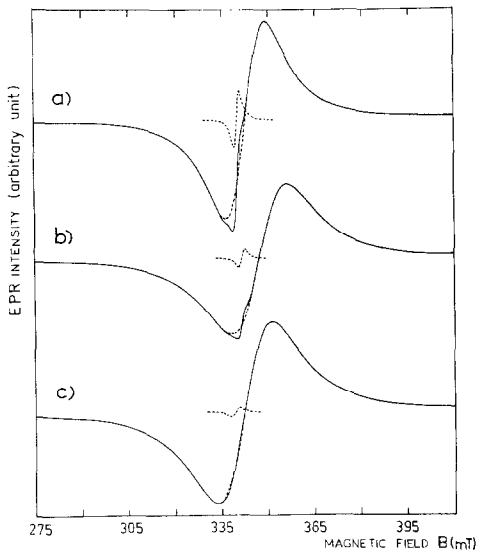

FIG. 5. EPR spectra of SGP bronzes: (a) powder, (b) film; the magnetic field B is parallel to the film surface. (c) Film; B is perpendicular to the film surface. This figure also shows the decomposition of the spectrum into a sum of two Lorentzian lines (dashed lines). The spectra have been recorded at $T = 140$ and 110 K for the powder and the film, respectively.

the following. The contribution $\langle\omega_{dip}^2\rangle \tau_c$ to the linewidth is proportional to $\Sigma_{i\neq j}[(1 + \cos^2\theta_{ij})/r_{ij}^6]$, where r_{ij} is the distance between the i^{th} and the j^{th} polarons, and θ_{ij} is the angle between r_{ij} and the magnetic field B. At low temperature, i.e., below 20–30 K, all the bipolarons at V_1 sites are in the singlet state and thus only polarons at V_3 sites contribute to the EPR spectrum. Since the concentration of these polarons is temperature independent, the distances r_{ij} between polarons, and hence the EPR linewidth, should be constant below 20–30 K. At higher temperatures, the bipolarons dissociate into isolated polarons at V_1 sites. Consequently the concentration of polarons should increase and the distance r_{ij} should decrease with increasing temperature. The result is an increase of the EPR linewidth, which should vary with the population of the polarons at V_1 sites. A rough estimate of the variation of the experimental linewidth ΔB_{av} for powder or films is thus given by the expression:

$$\Delta B_{av} = a + b \exp(-\Delta/kT)/[1 + \exp(-\Delta/kT)], \quad (2)$$

where the a parameter includes the contribution of unresolved hyperfine (hf) interactions in polarons, the contribution of dipolar interactions between polarons at V_3 sites and also the contribution of the anisotropy of the g tensor. The b term also includes contributions of hf interaction, of dipolar interactions of the types V_1–V_1 and V_1–V_3, and also the contribution of the anisotropy of the g tensor of polarons at V_1 sites. Figs. 6 and 7 show the temperature dependence of the EPR linewidth for SGP bronze powder and film, respectively. The data are fitted to expression (2) by using the value Δ/k measured by magnetic susceptibility measurements. The a parameter is the linewidth measured at liquid helium temperature, and the b parameter is adjusted to obtain the best fit. Examination of Figs. 6 and 7 shows that there is a good agreement between experimental and calculated linewidth in the

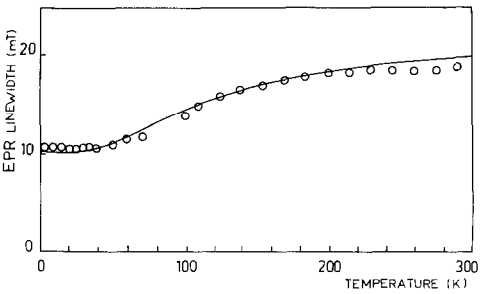

FIG. 6. Temperature dependence of the EPR linewidth of SGP bronze powder. The full line represents the variation calculated using expression (2) with a = 10.2 mT and b = 27.6 mT.

temperature range 4 to 180 K for both powder and film. However, at $T > 180$ K, the experimental linewidth is significantly smaller than the calculated one. This discrepancy may originate from phenomena not taken into account in the temperature dependence of the EPR linewidth:

(i) The increase of the polaron concentration at high temperature may produce exchange interactions between polarons in ad-

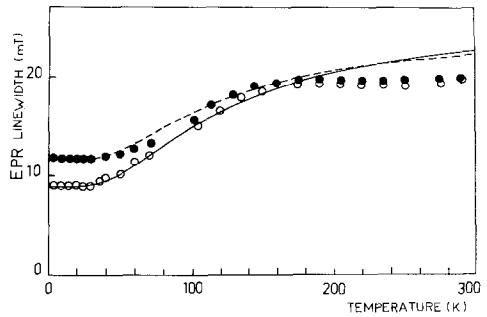

FIG. 7. Temperature dependence of EPR linewidth of SGP bronze film: empty circles and the full line represent the experimental and calculated variations when the magnetic field B is parallel to the film plane. Full circles and the dashed line represent the experimental and calculated variation when B is perpendicular to the film plane. The full line and the dashed line were calculated using expression (2) with a = 9 mT, b = 40.6 mT and a = 11.8 mT, b = 31.8 mT, respectively.

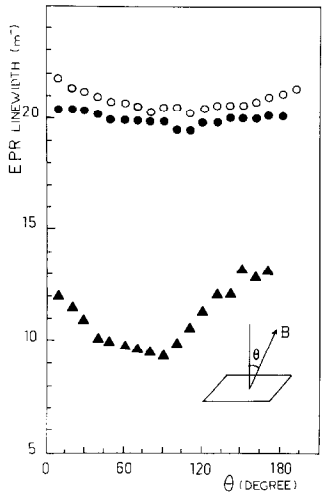

FIG. 8. Variation of the EPR linewidth with the angle between the magnetic field plane and the direction perpendicular to the film plane. Open circles: T = 290 K. Full circles: T = 200 K. Triangles: T = 14 K.

dition to the dipolar interactions, which can result in a narrowing of the EPR line. In this case, the parameters a and b should be temperature dependent.

(ii) The angular anisotropy of the EPR linewidth is also temperature dependent, as shown in Fig. 8 for SGP bronze film. This anisotropy is much more pronounced at low temperature, and its reduction at high temperature may be due to a decrease of the g factor anisotropy, produced, for example, by the exchange or by the rapid motion of the polarons. Since the g factor anisotropy is included in a and b parameters, its reduction with temperature should result in a reduction of the a and b parameters at high temperatures.

Electrical Conductivity

Conductivity measurements made on sintered samples or single crystals of the SSR bronze have shown that the bronze is a very good conductor. The conductivity along the b axis is $10^2\ \Omega^{-1} \cdot \mathrm{cm}^{-1}$ at 300 K and is higher by about two orders of magnitude than the conductivity in the (a,c) plane (*10*). This high conductivity was explained in terms of collective motion of bipolarons along the zig–zag chain between V_1 sites (*24, 25*). In the direction perpendicular to b, the hopping occurs in a quasi-one-dimensional fashion along V_1–V_3–$V_{3'}$–$V_{1'}$ chains.

For the SGP bronze, the temperature dependence, i.e., $\log \sigma T = f(1/T)$, of the conductivity $\sigma_\parallel$ ((a,b) plane) and $\sigma_\perp$ (c direction) is shown in Fig. 9. The evolution of $\sigma_\parallel$ versus T shows two types of behaviors:

(i) the "high temperature" domain above T = 100 K, where $\sigma_\parallel$ is of the Arrhenius type with an activation energy $W_\parallel$ = 0.07 eV.

(ii) the "low temperature" domain below 100 K, where the activation energy $W_\parallel$ decreases with the temperature.

In the high temperature domain, all phonon spectra take place in the thermal-activated hopping phenomena of the electrons above $T = \Theta_D/2$ = 100 K (*26*), where Θ_D = 200 K is the Debye temperature. In the low temperature domain ($T < \Theta_D/2$), the phonon spectra freezes progressively and one can observe a progressive decrease of the activation energy.

The value of the Debye temperature, Θ_D = 200 K, is in good agreement with previous studies on SSR bronze (Θ_D = 189 K) (*13*). The activation energy W = 0.07 eV is

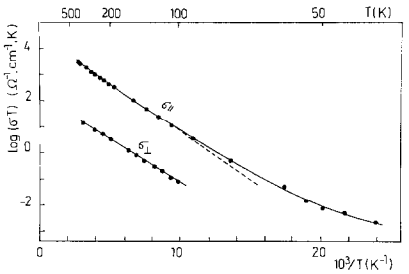

FIG. 9. Inverse temperature dependence of the SGP bronze electrical conductivity, $\log(\sigma T) = f(10^3/T)$. $\sigma_\parallel$ and $\sigma_\perp$ represent respectively the conductivities parallel and perpendicular to the film plane.

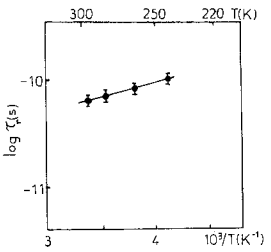

FIG. 10. Inverse temperature dependence of dielectric relaxation time τ_r due to electron hopping along the c-direction in SGP bronze.

the same as that found in SSR bronze (*10, 24, 27*), where $0.05 < W < 0.09$ eV depends on the synthesis method (single crystal, sintered powder, . . .) At $T = 300$ K, $\sigma_\parallel$ and $\sigma_\perp$ in SGP bronzes are respectively 8 $\Omega^{-1} \cdot cm^{-1}$ and 4.10 $^{2}\Omega^{-1} \cdot cm^{-1}$, with an anisotropy $\sigma_\parallel/\sigma_\perp = 200$. However, the conductivity parallel to the plane surface is the combination of the conductivities in the b and in the a directions. In fact, this value is an average value of σ_b and σ_a (with $\sigma_a \ll \sigma_b$). Thus $\sigma_\parallel$ may be approximated by $\sigma_\parallel = (\sigma_b + \sigma_a)/2$ ($\sigma_a \simeq \sigma_c$ corresponding to $\sigma_\perp$, see Fig. 9). Therefore the conductivity in the b direction for SGP bronze is $\sigma_b = 16$ $\Omega^{-1} \cdot cm^{-1}$ and is in the same order of magnitude as that found in the SSR bronze, i.e., $10 < \sigma < 100$ $\Omega^{-1} \cdot cm^{-1}$ (*10, 24, 27*).

The conductivity of β-$Na_{0.33}V_2O_5$ is due to an electron hopping motion in the zig–zag chains of vanadium ions along the b axis and in the sequence V_1–V_3–$V_{3'}$–$V_{1'}$ (a,c plane). We can interpret the experimental results of the electrical conductivity on the basis of the characteristic time, τ_c, of the electron hopping motion in SGP bronze. Recently, we have shown in a broad frequency range 1 MHz–10 GHz, one dielectric relaxation due to electron hopping along the c direction (V_1–V_3–$V_{3'}$–$V_{1'}$ sequence in projection on the c axis) on SGP bronze (*3*). Figure 10 shows that the temperature dependence of the dielectric relaxation time, τ_r, is of the Arrhenius type, i.e., $\tau_r = \tau_c \cdot \exp(W_h/kT)$, where $\tau_c = 10^{-11}$ sec and $W_h = 0.05$ eV are respectively the characteristic time for electron hopping between V_1 and $V_{3'}$ and the activation energy required for the hopping between V_3 and $V_{3'}$ (cf. Fig. 1). These results are in good agreement with those of Refs. (*24, 25*) and with conductivity measurements on single crystals of SSR bronze. The discrepancy between activation energies of dc-conductivity ("long-range" conductivity) $W = 0.07$ eV and of electron hopping ("local" conductivity) $W = 0.05$ eV is probably due to grain boundaries in the sample pellet. The conductivity along the c axis, σ_c, is due to an electron hopping motion and can be determined in terms of diffusive conduction by the expression:

$$\sigma_c T = N_c\,[(el_c)^2/k]\,\tau_c^{-1}\exp(-W_c/kT),$$

where l_c corresponds to the projection of the hopping distance l ($l = 9.3$ Å) among V_1–V_3–$V_{3'}$–$V_{1'}$, and N_c is the carrier concentration of a single electron having charge $-e$. N_c is expressed as:

$$N_c = N_0/6\,\{0.84\exp(-\Delta/kT)/[1 + \exp(-\Delta/kT)] + 0.16\},$$

where N_0 is the number of vanadium ions.

Assuming that $\tau_c = 10^{-11}$ sec, $W_c = 0.07$ eV, and $\Delta/k = 169$ K, it is found that the static conductivity along the c axis is on the order of 5.5×10^{-2} $\Omega^{-1} \cdot cm^{-1}$. This calculated value has the same order of magnitude as the measured value $\sigma_c = 4.10^{-2}$ $\Omega^{-1} \cdot cm^{-1}$ on the SGP bronze film.

However, it was not possible to study the hopping motion of the electrons in the film plane (a,b plane) by the dielectric relaxation technique because of the existence of a skin effect for frequencies above 2 GHz. This phenomenon is a consequence of the high conductivity in the (a,b) plane, i.e., $\sigma_\parallel = 8$ $\Omega^{-1} \cdot cm^{-1}$ at 300 K. The conductivity along the b axis is expressed as:

$$\sigma_b T = N_h[(el_h)^2/k]\,\tau_c^{-1}\exp(-W_h/kT).$$

Following previous works (*24, 25*), if we

consider the same characteristic time τ_c along the b axis rather than along the perpendicular direction, i.e., $\tau_c = 10^{-11}$ sec, and taking $l_b = 3.6$ Å and the experimental conductivity value $\sigma_b = 16\,\Omega^{-1} \cdot cm^{-1}$ with $W_b = 0.07$ eV, we obtain $N_b = 13\,N_0$. This result means that 20 bipolarons move at the same time collectively in SGP bronze, in the same way as the SSR bronze (*24*). The activation energy $W_b = 0.07$ eV required for the collective hopping motion of the bipolarons in phase in the SGP bronze should be due to the pinning energy of the bipolaronic state domain wall motion, as in the case of the SSR bronze.

Conclusion

The experimental results obtained by magnetic susceptibility and EPR techniques have shown that the bipolaron model (*13*) can be applied to the bronze β-$Na_{0.33}V_2O_5$ synthesized by the sol–gel process. We have demonstrated that the electronic properties are not modified by the new synthesis method. In relation to structural studies, which have shown that the SGP films are orientated, the electrical properties are strongly anisotropic (anisotropy degree ≈ 200–300). Consequently, it is thus possible to obtain by the sol–gel process a material with properties of a nearly "single-crystal" type. However, it should be necessary to study also the dynamical properties of electronic transfer along the b axis by dielectric relaxation techniques (e.g., correlation time τ_c of electron hopping between V_I sites) for a complete comparison between the two kinds of bronzes. A study of the electrical conductivity behavior above room temperature is under investigation.

References

1. L. Znaidi, N. Baffier, and M. Huber, *Mater. Res. Bull.* **24,** 1501 (1989).
2. J. P. Pereira-Ramos, L. Znaidi, N. Baffier, and R. Messina, *Solid State Ionics* **28–30,** 886 (1988).
3. J. C. Badot and N. Baffier, *J. Sol. State Chem.* submitted for publication.
4. P. Hautefeuille, *C.R. Acad. Sci.* **90,** 744 (1880).
5. J. Galy, M. Pouchard, A. Casalot, and P. Hagenmuller, *Bull. Soc. Fr. Min. Cristall.* **XC,** 544 (1967).
6. P. Hagenmuller, *in* "Non Stoichiometric Compounds, Tungsten Bronzes, Vanadium Bronzes and Related Compounds," (D. J. Bevan and P. Hagenmuller, Eds.), Vol. 1, 569, Pergamon Press, Oxford (1973).
7. P. Hagenmuller, XXIIth Congress IUPAC, Sydney, 67 (1969).
8. J. Galy, J. Darriet, A. Casalot, and J. B. Goodenough, *J. Sol. State Chem.* **1,** 339 (1970).
9. J. B. Goodenough, *J. Solid State Chem.* **1,** 349 (1970).
10. J. H. Perlstein and J. Sienko, *J. Chem. Phys.* **48,** 174 (1968).
11. Y. Kanaï, S. Kagoshima, and H. Nagasawa, *J. Phys. Soc. Japan,* **51,** 697 (1982).
12. M. Onoda, T. Takahashi, and H. Nagasawa, *Phys. Status Solidi B* 109, 793 (1982).
13. B. K. Chakraverty, M. J. Sienko, and J. Bonnerot, *Phys. Rev. B* 17, 3781 (1978).
14. T. Takahashi and H. Nagasawa, *Solid State Commun.* **39,** 1125 (1981).
15. H. Nagasawa, T. Erata, and H. Suzuki, *J. Magn. Magn. Mater.* **52,** 2231 (1983).
16. P. Aldebert, N. Baffier, N. Gharbi, and J. Livage, *Mater. Res. Bull.* **16,** 669 (1981).
17. J. J. Legendre and J. Livage, *J. Coll. Int. Sci.* **94**(1), 75 (1983).
18. H. G. Bachman, F. R. Ahmed, and W. H. Barnes, *Zeit. Krist.* **115,** 110 (1961).
19. A. Bouhaouss, P. Aldebert, N. Baffier and J. Livage, *Rev. Chim. Mineral.* **22,** 417 (1985).
20. L. Znaidi, N. Baffier, and D. Lemordant, *Solid State Ionics* **28–30,** 1750 (1988).
21. L. Znaidi, Thèse Université Paris VI (1989).
22. J. C. Badot, A. Fourrier-Lamer, N. Baffier, *J. Physique* **46,** 2107 (1985).
23. J. C. Badot, A. Fourrier-Lamer, N. Baffier, and Ph. Colomban, *J. Physique* **48,** 1325 (1987).
24. H. Nagasawa, T. Erata, *J. Physique* **43,** C3-1737 (1983).
25. T. Erata and H. Nagasawa, *J. Phys. Soc. Japan* **52,** 3652 (1983).
26. T. Holstein, *Ann. Physics* **8,** 325, 343 (1959).
27. V. K. Kapustkin, V. L. Volkov, and A. A. Fotiev, *J. Solid State Chem.* **19,** 359 (1976).